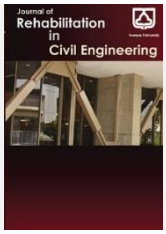

Journal of Rehabilitation in Civil Engineering

Journal homepage: https://civiljournal.semnan.ac.ir/

Best Location of Conventional Outrigger in Tall Buildings with Discontinuity in Moment of Inertia of Shear Core using Energy Method with Closed-Form Solution

Hamed Fallahi [1]; Reza Rahgozar [2,*]; Yasser Sharifi [3]

1. Ph.D. Candidate, Faculty of Engineering, Shahid Bahonar University of Kerman, Kerman, Iran
2. Professor, Faculty of Engineering, Shahid Bahonar University of Kerman, Kerman, Iran
3.Professor, Faculty of Engineering, Vali-e-Asr University of Rafsanjan, Rafsanjan, Iran
* Corresponding author: *rahgozar@uk.ac.ir*

ARTICLE INFO

Article history:
Received: 04 June 2025
Revised: 12 October 2025
Accepted: 21 November 2025

Keywords:
Tall building;
Conventional outrigger;
Discontinuity in shear core.

ABSTRACT

This study presents a graphical solution for determining the initial positioning of Conventional Outrigger (CO) system in the shear core with discontinuity in moment of inertia, using the energy method in tall building. In this model a cantilevered beam presents The framed-tube system, while the CO system is modeled by rotational springs located at their respective positions. By applying the energy method, best locations of the CO are identified along the building height to maximize energy absorption and dissipation. For validation, the model is compared with the case of a uniform shear core, and the results are shown to be consistent with previous studies. Quantitative results indicate that when the shear core has no discontinuity, the best positions of the CO are approximately 0.44L, 0.49L, 0.32L, and 0.52L of the building height (L) for uniform, triangular, inverted triangular, and parabolic load distributions, respectively. Furthermore, with increasing values of the parameter γ, which corresponds to greater slenderness in the second segment of the shear core, the best positions shift upward along the building height. In some cases, the best location falls within the first segment of the shear core, similar to the case of a uniform shear core. The proposed closed-form solution and the developed utility graphs offer a practical and efficient tool for identifying the initial positioning of CO system during the preliminary design of tall buildings.

E-ISSN: 2345-4423

How to cite this article:
Fallahi, H. , Rahgozar, R. and Sharifi, Y. (2026). Best Location of Conventional Outrigger in Tall Buildings with Discontinuity in Moment of Inertia of Shear Core using Energy Method with Closed-Form Solution. (2337). Journal of Rehabilitation in Civil Engineering, 14(3), 2337 https://doi.org/10.22075/jrce.2025.2337

List of symbols

C Constant for triangular and inverted triangular distributed load
CO Conventional outrigger
c_1 Integration constants
c_2 Integration constants
c_3 Integration constants
c_4 Integration constants
E Energy function
E(x) Function of Young's modulus
E_0 Modulus of elasticity
I(x) Function of moment of inertia
I_0 Moment of inertia
I_{eq} Equal moment of inertia
k Stiffness of spring
L Total height of the core
M(x) Function of bending moment
M_o Moment that was created by CO
q(x) Function of external load
u(x) Function of displacement
U(x) Heaviside function
V(x) Function of shear core
w Constant for uniform and parabolic distributed load
x Location of CO
x_o Location of discontinuity of moment of inertia in shear core
γ Constant for reduction of moment of inertia in core
$\chi(x)$ Function of beam curvature
$\varphi(x)$ Function of slope
$\theta(x)$ Rotation angle

1. Introduction

The concept of belt truss and conventional outrigger (CO) system in high-rise buildings has been utilized as a lateral load resistance system for over 50 years. Determining the best location of lateral load resistance systems is an important issue [1]. Use of CO system to resist earthquakes and wind loads in tall buildings has become very common for the purpose of reducing structural displacement and increasing lateral load resistance. The shear core is one of the main lateral load-resistance systems in tall buildings [2]. The effectiveness of CO system in reducing displacement and drift was found to be highly dependent on location of it in structures height [3]. The best position for a CO system has been determined by Smith and Salim [4] and Smith and Coull [5], to be at 0.45 height from the top of the structure using the displacement method. Wu and Lee [6] investigated the relationships proposed by Smith and Salim [4] and Smith and Coull [5], and developed an additional graph for triangular distributed load. Furthermore, Baygi and Khazaee [7] expand the relationships for the concentrated load. Throughout all of these studies, as the CO's flexibility increases, the CO's position moves toward the top of the structure. Multi-objective optimization algorithms are used in tall buildings [8–11]. Chen and Zhang's proposed the location of CO by genetic algorithm and reducing both the top displacement and base moment of the structure [9]. They presented different positions

that effectively mitigate the top displacement and base moment. Park et al. [12] suggested the position of one and two COs system to be at 0.39 and 0.27, and 0.59 height from the top of the building using a weight reduction function. Habrah et al. [13] studied the CO position in the shear core under uniform, triangular, and parabolic distributed loads. They presented a position of 0.59 for one CO and 0.35 and 0.73 for two COs under parabolic load from the building's base.

A study shows using a frame tube and shear wall system is a highly effective method for reducing horizontal displacements in tall buildings. Obtaining the natural frequency of tall buildings has been investigated by some researchers [14] . A continuous model and separation of variables method have been used to determine the building's natural frequency based on the energy method [15]. Kwan [16] presented a simplified technique for calculating horizontal displacements in a frame tube system using third and second-degree functions. Rahgozar et al. [17] added a rigid CO and incorporated Kwan's [16] relations to establish the relationships between lateral displacement and CO, ultimately determining the best point for the CO. They validated the presented relationships and found them to be very close to reality. To minimize error in the proposed model, Rahgozar et al. [18] introduced fourth and fifth-degree approximation functions for the shear stiffness in the flange and web of the frame tube with CO, resulting in more precise relationships than previous research.

Kamgar and Rahgozar [19] have presented relations for the shear core with linear moment of inertia and provided functional graphs with dimensionless variables to ascertain the CO position, which is located at 0.44 from the base of the structure for a rigid CO under uniform distributed load. Also Some functional graph for uniform moment of inertia have been presented [20]. In addition to new systems, a CO is always necessary in a structure due to a CO can prevent the risk of collapse [21]. The practice of CO along belt truss structure in high rise construction Increases stiffness and build structure effective to sustain loads which acts laterally. COs with belt truss is more effective for high rise building considering maximum story displacement and drift [22]. In Table 1, different methods of determining best location of CO system are summarized.

Table 1. Different methods of determining best location of CO system.

Researchers	Lateral load	Shape of shear core	Method
Smith and Salim [4], Smith and Coull [5]	Uniform	Uniform	Reduce top displacement
Wu and Lee [6]	Triangular	Uniform	Reduce top displacement
Baygi and Khazaee [7]	Concentrated Load at the top of structure	Uniform	Reduce top displacement
Chen and Zhang [9]	Uniform	Uniform	Reduce top displacement and base moment
Park et al. [12]	Uniform	Uniform	Reduce weight of structure
Habrah et al.[13]	Uniform, triangular, parabolic	Uniform	Reduce top displacement
Kamgar and Rahgozar [19]	Uniform, triangular, Concentrated Load at the top of structure	Linear	Maximize energy function
Kamgar and Rahgozar [20]	Uniform, triangular, Concentrated Load at the top of structure	Uniform	Maximize energy function

According to Table 1, in this paper, the energy method and close form solution is used to determine the best location of CO systems in a tall building with discontinuity in shear core. For this purpose, a tall building consisting of a framed tube, shear core, CO system is considered. Then, the continuum approach is used to model the framed tube system as a cantilevered beam with a box cross section. The CO systems are modeled by rotational springs placed at their locations. The practical graphs presented for four types of static lateral loadings, uniform, triangular, inverted triangular, and parabolic loads along the structure’s height.

2. Research significance

This research introduces a closed-form energy-based solution to determine the best placement of CO systems in tall buildings with discontinuity in shear cores. Unlike conventional studies that often neglect discontinuities, the proposed method provides utility graphs for different lateral loading patterns, offering a practical tool for preliminary design. By reducing computational effort while improving accuracy, the study bridges a gap in current literature and delivers direct practical value for optimizing the seismic and structural performance of tall buildings. Flowchart for determined the best location of CO system based on energy method has drawn in Figure 1.

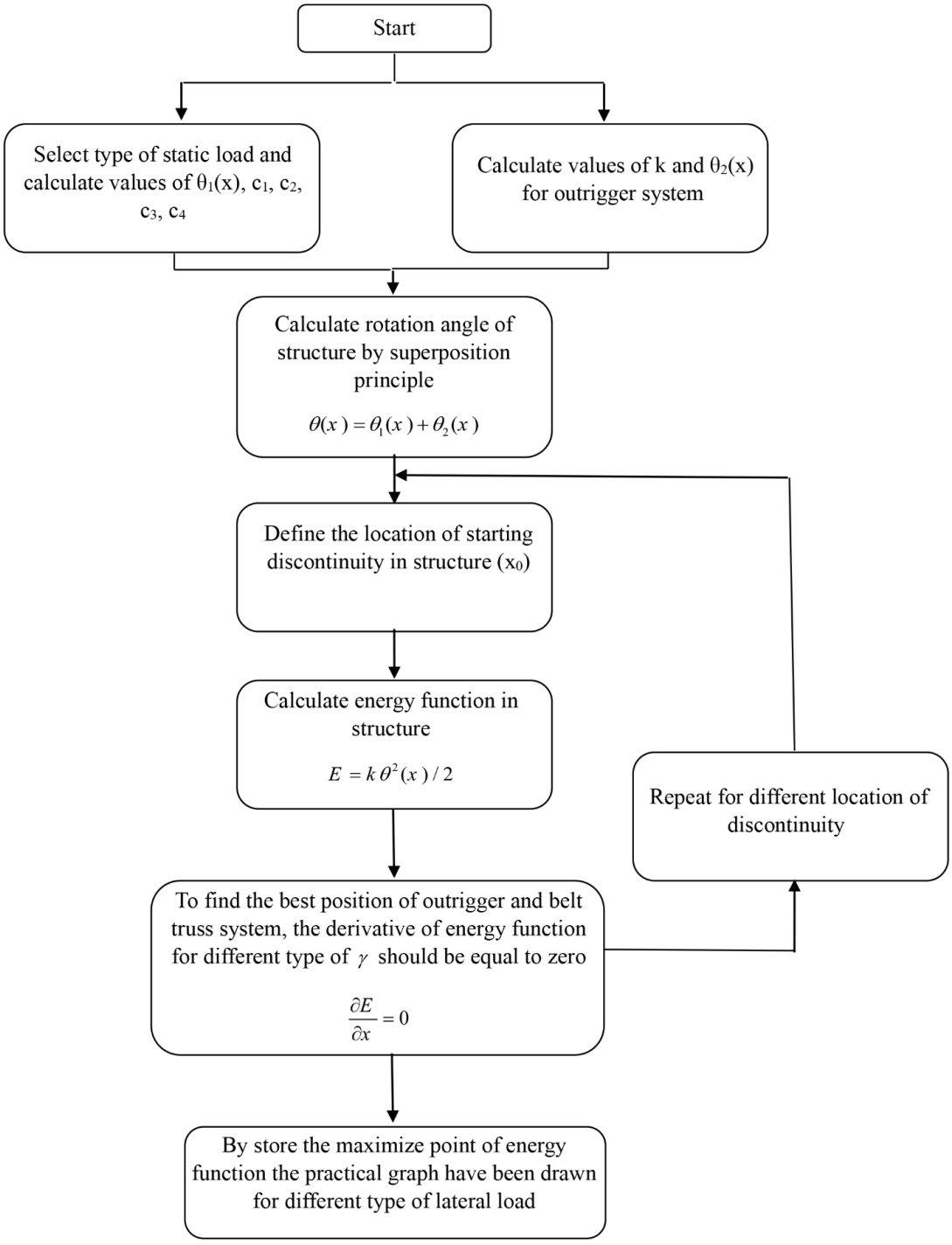

Fig. 1. Flowchart for determined the best location of CO system.

3. Hypothesis and program formulation

In this study, the CO position has been suggested by energy method with closed-form solution. The following assumptions were applied:

1) The connection of the CO allows only axial forces to be transmitted.

2) The CO is rigidly connected to the shear core.

3) The belt truss is rigid.

4) The axial stiffness of the exterior columns is constant and uniform in height.

5) The shear core has a discontinuity in the moment of inertia and the location of the CO is in the second section of the shear core.

6) The equal moment of inertia (I_{eq}) is assumed in obtaining the rotation angle of the CO.

In this article, continuous modeling is used for tall buildings, which has the advantages of reducing the degrees of freedom and easier extraction of equations. As shown in Figure 2, the CO has been replaced by a rotational spring. The resulting moment of rotational spring act in the opposite direction of the internal moment of the shear core, which reduces the internal moment and displacement of the shear core. The energy criterion for calculating the initial location of CO is expressed as follows: When the structure is subjected to external loads, work is done on the structure by the external load. The work of external forces is stored in the members as strain energy. when the energy absorbed by the spring is maximized, the spring is in the best position.

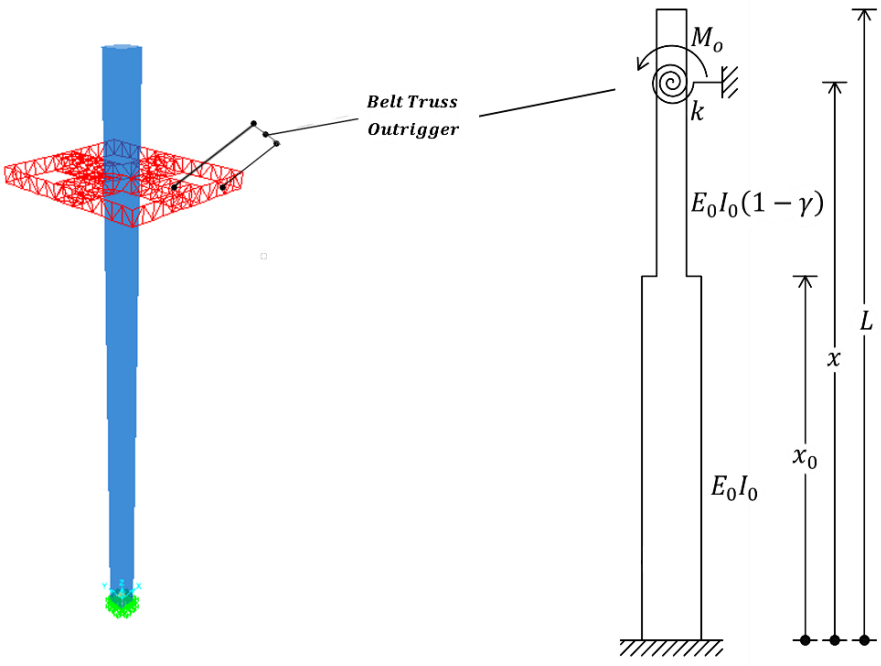

Fig. 2. Schematic modeling of CO system in a tall structure.

4. Theories

4.1. Energy theory

Assuming a CO modeled as a spring and $E = k\theta^2(x)/2$ present the energy stored in it. Referring to Figure 3, if the spring is positioned at a distance x from the base of the structure, it becomes necessary to determine

its best location. In this research, four different types of lateral loading are considered for the structure as shown in Figure 3.

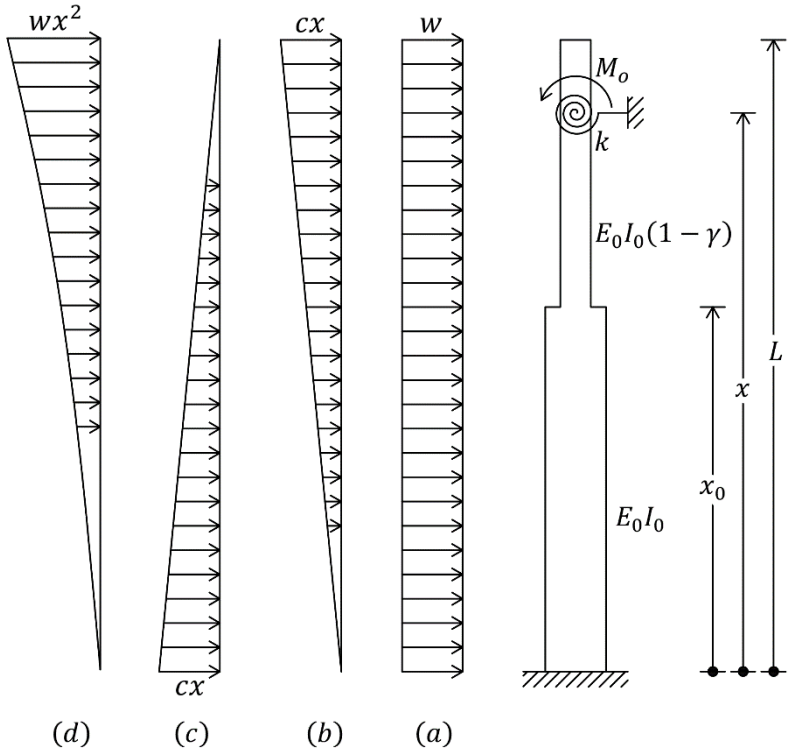

Fig. 3. Types of lateral loads along the building's height (a) uniform , (b) triangular , (c) inverted triangular , (d) parabolic distributed load.

4.2. Slope in beam with flexural discontinuity

A closed-form solution for the Euler-Bernoulli beam with discontinuity has been introduced by Biondi and Caddemi [23]. The static equations of the Euler-Bernoulli beam are as follows:

$$V'(x) = -q(x) \quad (1)$$
$$\mathrm{M'(x) = V(x)} \quad (2)$$
$$\chi(\mathrm{x}) = \frac{\mathrm{M(x)}}{\mathrm{E(x)I(x)}} \quad (3)$$
$$\chi(\mathrm{x}) = \varphi'(\mathrm{x}) \quad (4)$$
$$\varphi(\mathrm{x}) = -\mathrm{u'(x)} \quad (5)$$

In Eqs. (1-5), $q(x)$, $V(x)$, $M(x)$, $u(x)$, $\varphi(x)$, $\chi(x)$, $E(x)$ and $I(x)$ represent the function of external load, shear force, bending moment, displacement, slope, beam curvature, Young's modulus, and member's moment of inertia respectively. The prime symbol ($'$) represents the derivation respect to the coordinates x in the interval $[0 - \mathrm{L}]$. By combining Eqs. (3)-(5) the following equation has been obtained:

$$\mathrm{E(x)I(x)u''(x) = -M(x)} \quad (6)$$

According to Eqs. (1) and (2), the fourth-degree Euler-Bernoulli equation has been expressed as follows:

$$\mathrm{[E(x)I(x)u''(x)]'' = q(x)} \quad (7)$$

The Heaviside function is used to show sudden changes in Young's modulus or moment of inertia or both:

$$\mathrm{E(x)I(x) = E_0I_0[1 - \gamma U(x - x_0)]} \quad (8)$$

In Eq. (8), $\mathrm{U(x - x_0)}$ represents the Heaviside function and $\mathrm{x_0}$ indicates the starting point of bending stiffness changes. By substituting Eq. (8) into Eq. (7):

$$\mathrm{[E_0I_0(1 - \gamma U(x - x_0))u''(x)]'' = q(x)} \quad (9)$$

According to the physics of the problem, the bending stiffness of the beam should not be negative, which is necessary for condition $\gamma \leq 1$ specified in Eq. (9). By integrating twice from Eq. (9):

$$u''(x) = \frac{1}{E_0 I_0 (1-\gamma U(x-x_0))}(b_1 + b_2 + q^{[2]}(x)) \quad (10)$$

In Eq. (10), $q^{[2]}(x)$ represents the double integration of the load function. With an algebraic simplification, Eq. (10) can be rewritten:

$$\chi(x) = -u''(x) = -\left(2c_3 + 6c_4 x + \frac{q^{[2]}(x)}{E_0 I_0}\right)\left(1 + \frac{\gamma}{1-\gamma}U(x-x_0)\right) \quad (11)$$

The constants of Eq. (11) have been defined as follows:

$$c_3 = \frac{b_1}{2E_0 I_0} \quad (12)$$

$$c_4 = \frac{b_2}{6E_0 I_0} \quad (13)$$

By integrating Eq. (11), the slope function has been obtained as follows:

$$\varphi(x) = -u'(x) = -c_2 - 2c_3\left[x + \frac{\gamma}{1-\gamma}(x-x_0)U(x-x_0)\right]$$
$$-3c_4\left[x^2 + \frac{\gamma}{1-\gamma}(x^2 - x_0^2)U(x-x_0)\right]$$
$$-\frac{q^{[3]}(x)}{E_0 I_0} - \frac{\gamma}{1-\gamma}\frac{q^{[3]}(x) - q^{[3]}(x_0)}{E_0 I_0}U(x-x_0) \quad (14)$$

By integrating Eq. (14), the closed-form solution of the displacement function has been obtained as follows:

$$u(x) = c_1 + c_2 x + c_3\left[x^2 + \frac{\gamma}{1-\gamma}(x-x_0)^2 U(x-x_0)\right]$$
$$+c_4\left[x^3 + \frac{\gamma}{1-\gamma}(x^3 - 3x_0^2 x + 2x_0^3)U(x-x_0)\right]$$
$$+\frac{q^{[4]}(x)}{E_0 I_0} + \frac{\gamma}{1-\gamma}\frac{q^{[4]}(x) - q^{[4]}(x_0) - q^{[3]}(x_0)(x-x_0)}{E_0 I_0}U(x-x_0) \quad (15)$$

In Eq. (15) c_1, c_2, c_3, and c_4 are integration constants obtained from the boundary conditions. The moment function can be expressed by using Eqs. (8) and (11) as follows:

$$M(x) = E(x)I(x)\chi(x) = -E_0 I_0\left(2c_3 + 6c_4 x + \frac{q^{[2]}(x)}{E_0 I_0}\right) \quad (16)$$

By differentiating Eq. (16), the shear function has been obtained as follows:

$$V(x) = M'(x) = -E_0 I_0\left(6c_4 + \frac{q^{[1]}(x)}{E_0 I_0}\right) \quad (17)$$

4.3. Equivalent moment of inertia

Since the Biondi and Caddemi [23] have not provided a model for concentrated moment or concentrated loads within the structure, the equivalent moment of inertia for a shear core has been used to simulate the effect of the CO. Eq. (17) represents the equivalent moment of inertia for a beam with discontinuity in the moment of inertia (Figure 4) [24].

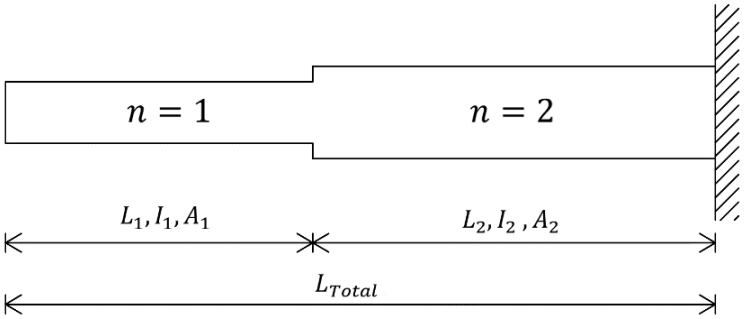

Fig. 4. The cantilever stepped beam [24].

$$I_{eq} = \frac{(L_{Total})^3}{\left[\frac{(L_1)^3}{I_1} + \frac{(L_{Total})^3 - (L_1)^3}{I_2}\right]} = \frac{(L_{Total})^3}{\sum_{n=1}^{2}\left[\frac{(L_n)^3 - (L_{n-1})^3}{I_n}\right]} \quad (18)$$

In Eq. (18), L_{Total},L_1,L_2,A_1,A_2,$I_1$and I_2have been defined to represents the total length of the beam, length of the first part, length of the second part, cross section of the first part, cross section of the second part, the moment of inertia of the first part, and moment of inertia of the second part, respectively.

5. Discussion and results

The superposition principle has been applied to determine the rotation angle, as shown in Figure 5:

$$\theta(x) = \theta_1(x) + \theta_2(x) \quad (19)$$

In Eq. (19), $\theta_1(x)$ is the rotation angle due to the uniform distributed load in the section with bending discontinuity and $\theta_2(x)$ is the rotation angle of CO system, which has been obtained as an equivalent moment of inertia.

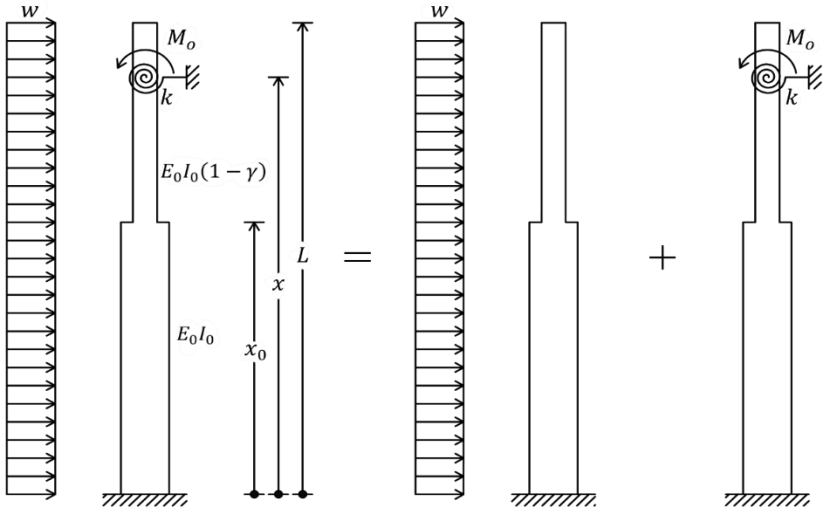

Fig. 5. Tall structure with a CO subjected to Superposition principle.

5.1. Uniform distributed load

The rotation due to the uniform distributed load has been obtained from Eq. (14). The constant of Eq. (14) has been determined using boundary conditions. The Constants c_1 and c_2 have been obtained zero by applying boundary conditions $u(0) = 0$,$\varphi(0) = 0$ and by considering $M(0) = 0$ and $V(0) = 0$ in Eqs. (16) and (17):

$$c_3 = \frac{wL^2}{4E_0I_0}, c_4 = -\frac{wL}{6E_0I_0} \quad (20)$$

As a result, $\theta_1(x)$ becomes:

$$\theta_1(x) = -\frac{wL^2}{2E_0I_0}\left[x + \frac{\gamma}{1-\gamma}(x - x_0)U(x - x_0)\right] + \frac{wL}{2E_0I_0}\left[x^2 + \frac{\gamma}{1-\gamma}(x^2 - x_0^2)U(x - x_0)\right] - \frac{q^{[3]}(x)}{E_0I_0} - \frac{\gamma}{1-\gamma}\frac{q^{[3]}(x) - q^{[3]}(x_0)}{E_0I_0}U(x - x_0) \quad (21)$$

For calculating the rotation angle for concentrated moment:

$$\theta(x) = \frac{1}{E_0I_{eq}}\int_0^x M(x)dx + \theta_0 \quad (22)$$

In Eq. (22) $I_{eq}$is the equivalent of the moment of inertia. Due to choosing the origin from the base of the structure$\theta_0 = 0$, and by Substituting $M_o = k\theta(x)$ in Eq. (22):

$$\theta_2(x) = -\frac{M_o x}{E_0 I_{eq}} = -\frac{k\theta(x)x}{E_0 I_{eq}} \quad (23)$$

Synthesizing Eqs. (19), (21) and (23):

$$\theta(x) = E_0 I_{eq}\left(-\frac{wL^2}{2E_0 I_0}\left[x + \frac{\gamma}{1-\gamma}(x-x_0)U(x-x_0)\right] + \frac{wL}{2E_0 I_0}\left[x^2 + \frac{\gamma}{1-\gamma}(x^2-x_0^2)U(x-x_0)\right] - \frac{q^{[3]}(x)}{E_0 I_0} - \frac{\gamma}{1-\gamma}\frac{q^{[3]}(x)-q^{[3]}(x_0)}{E_0 I_0}U(x-x_0)\right)/(E_0 I_{eq} + AEd^2/2) \quad (24)$$

The moment in the CO has been created by perimeter columns:

$$M_o = Pd \quad (25)$$

$$P = \frac{AE\delta}{x} \quad (26)$$

$$\theta_2(x) = \frac{2\delta}{d} \quad (27)$$

In Eqs. (25)-(27), AE represents the axial stiffness of the perimeter columns, and δ denotes the displacement of the perimeter columns due to the axial load. The Eq. (27) has been obtained by assuming a small rotational angle. By applying Eqs. (25)-(27), the equivalent stiffness of the rotational spring becomes:

$$k = \frac{AEd^2}{2x} \quad (28)$$

By substituting Eqs. (24) and (28) in $E = k\theta^2(x)/2$, the energy function stored in the CO has been obtained. By using Eq. (29), the best locations of the CO are obtained.

$$\frac{\partial E}{\partial x} = 0 \quad (29)$$

In Eq. (29) the position of the CO has been obtained by assuming $0.2 \le \gamma \le 0.9$ and $0.3L \le x_0 \le 0.8L$the graph shown in Figure 6 can be illustrated.

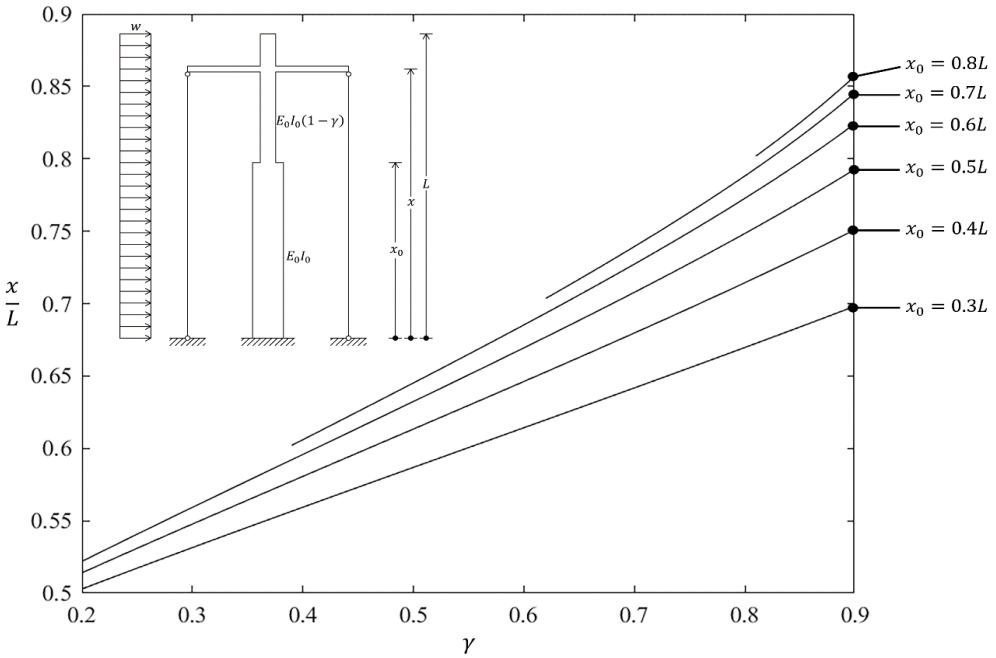

Fig. 6. Best position of CO system for uniform distributed loading.

In Eq. (24), assuming $x_0 = 0$ and solving Eq. (29), the position $x = 0.44L$ has been obtained for the CO, which is the position of the rigid CO with a uniform shear core [19,20,25,26]. The position of the CO varies between *0.5L* and *0.85L* for different points of bending discontinuity. By increasing the value of γ (which corresponds to an increase in the slenderness of the second part of the structure), the position of the CO shifts toward the top of the structure. In Figure 6 for some values of γ, the position of the CO is located in the first part of the shear core, in which case Eq. (24) reduces to:

$$\theta(x) = E_0 I_{eq}(-\frac{wL^2x}{2E_0I_0} + \frac{wLx^2}{2E_0I_0} - \frac{q^{[3]}(x)}{E_0I_0})/(E_0I_{eq} + AEd^2/2) \quad (30)$$

By replacing Eqs. (28) and (29) into Eq. (30), position of CO obtained to be 0.44L.

5.2. Triangular distributed load

The angle of rotation for triangular distributed load has been obtained from Eq. (14). By using the boundary conditions $u(0) = 0, \varphi(0) = 0, M(L) = 0$ and $V(L) = 0$ in Eqs. (14-17):

$$c_1 = 0, c_2 = 0, c_3 = \frac{cL^3}{6E_0I_0}, c_4 = -\frac{cL^2}{12E_0I_0} \quad (31)$$

Replacing Eq. (31) in Eq. (14), $\theta_1(x)$:

$$\theta_1(x) = -\frac{cL^3}{3E_0I_0}\left[x + \frac{\gamma}{1-\gamma}(x - x_0)U(x - x_0)\right] + \frac{cL^2}{4E_0I_0}\left[x^2 + \frac{\gamma}{1-\gamma}(x^2 - x_0^2)U(x - x_0)\right] - \frac{q^{[3]}(x)}{E_0I_0} - \frac{\gamma}{1-\gamma}\frac{q^{[3]}(x) - q^{[3]}(x_0)}{E_0I_0}U(x - x_0) \quad (32)$$

Synthesizing Eqs. (19), (23) and (32), it simplifies to:

$$\theta(x) = E_0I_{eq}(-\frac{cL^3}{3E_0I_0}\left[x + \frac{\gamma}{1-\gamma}(x - x_0)U(x - x_0)\right] + \frac{cL^2}{4E_0I_0}\left[x^2 + \frac{\gamma}{1-\gamma}(x^2 - x_0^2)U(x - x_0)\right] - \frac{q^{[3]}(x)}{E_0I_0} - \frac{\gamma}{1-\gamma}\frac{q^{[3]}(x) - q^{[3]}(x_0)}{E_0I_0}U(x - x_0))/(E_0I_{eq} + AEd^2/2) \quad (33)$$

Synthesizing Eqs. (29), (28) and (33), the graph shown in Figure 7 has been drawn for a triangular distributed load.

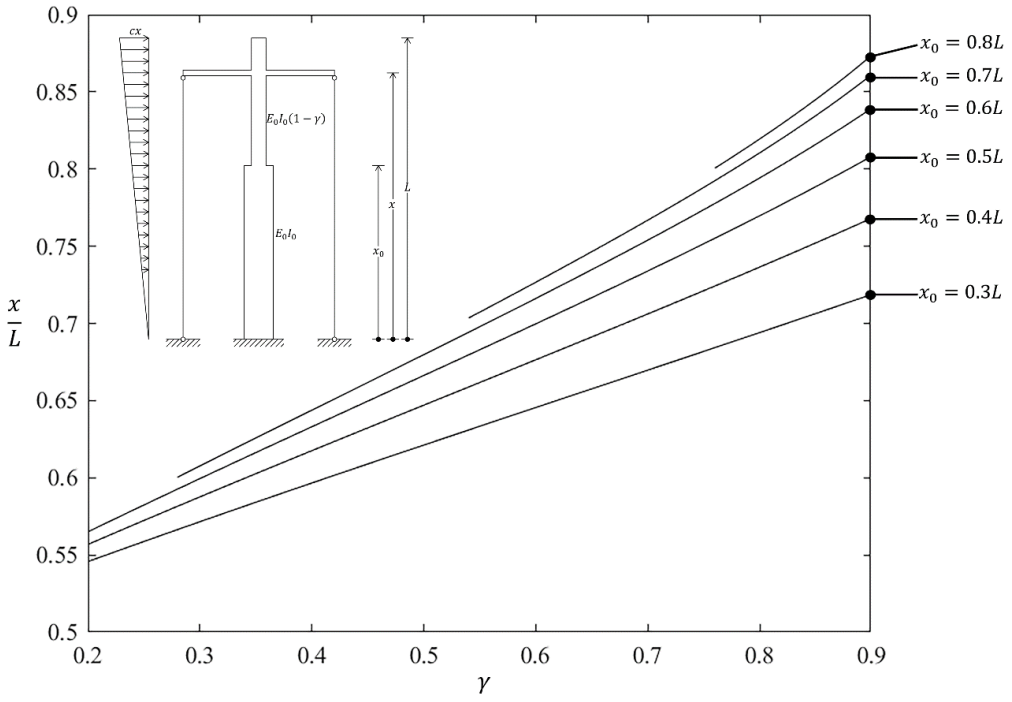

Fig. 7. Best position of CO system for a triangular distributed load.

In Eq. (33), assuming $x_0 = 0$ and solving Eq. (29), the position $x = 0.49L$ has been obtained for the CO, which is the exact position of the rigid CO with a uniform shear core [19,20,25,26]. The position of the CO varies between *0.54L* and *0.87L* for different points of bending discontinuity. By increasing the value of γ (which corresponds to an increase in the slenderness of the second part of the structure), the position of the

CO moves to the top of the structure. In Figure 7, for some values of γ, the position of the CO is located in the first part of the shear core, in which case Eq. (33) reduces to:

$$\theta(x) = E_0 I_{eq}\left(-\frac{cL^3 x}{3E_0 I_0} + \frac{cL^2 x^2}{4E_0 I_0} - \frac{q^{[3]}(x)}{E_0 I_0}\right)/(E_0 I_{eq} + AEd^2/2) \quad (34)$$

By replacing Eqs (28) and (34) in Eq. (29), position $0.49L$has been obtained.

5.3. Inverted triangular distributed load

By considering the boundary conditions in this type of loading, the coefficients of Eq. (14):

$$c_1 = 0, c_2 = 0, c_3 = \frac{cL^3}{6E_0 I_0}, c_4 = -\frac{cL^2}{12E_0 I_0} \quad (35)$$

By substituting Eq. (35) in Eq. (14), $\theta_1(x)$ can be expressed as:

$$\theta_1(x) = -\frac{cL^3}{3E_0 I_0}\left[x + \frac{\gamma}{1-\gamma}(x - x_0)U(x - x_0)\right] + \frac{cL^2}{4E_0 I_0}\left[x^2 + \frac{\gamma}{1-\gamma}(x^2 - x_0^2)U(x - x_0)\right] - \frac{q^{[3]}(x)}{E_0 I_0} - \frac{\gamma}{1-\gamma}\frac{q^{[3]}(x) - q^{[3]}(x_0)}{E_0 I_0}U(x - x_0) \quad (36)$$

By substituting Eqs. (23) and (36) in Eq. (19):

$$\theta(x) = E_0 I_{eq}\left(-\frac{cL^3}{3E_0 I_0}\left[x + \frac{\gamma}{1-\gamma}(x - x_0)U(x - x_0)\right] + \frac{cL^2}{4E_0 I_0}\left[x^2 + \frac{\gamma}{1-\gamma}(x^2 - x_0^2)U(x - x_0)\right] - \frac{q^{[3]}(x)}{E_0 I_0} - \frac{\gamma}{1-\gamma}\frac{q^{[3]}(x) - q^{[3]}(x_0)}{E_0 I_0}U(x - x_0)\right)/(E_0 I_{eq} + AEd^2/2) \quad (37)$$

Finally, by replacing Eqs. (28) and (37) into Eq. (29), the graph shown in Figure 8 has been drawn for the inverted triangular distributed load.

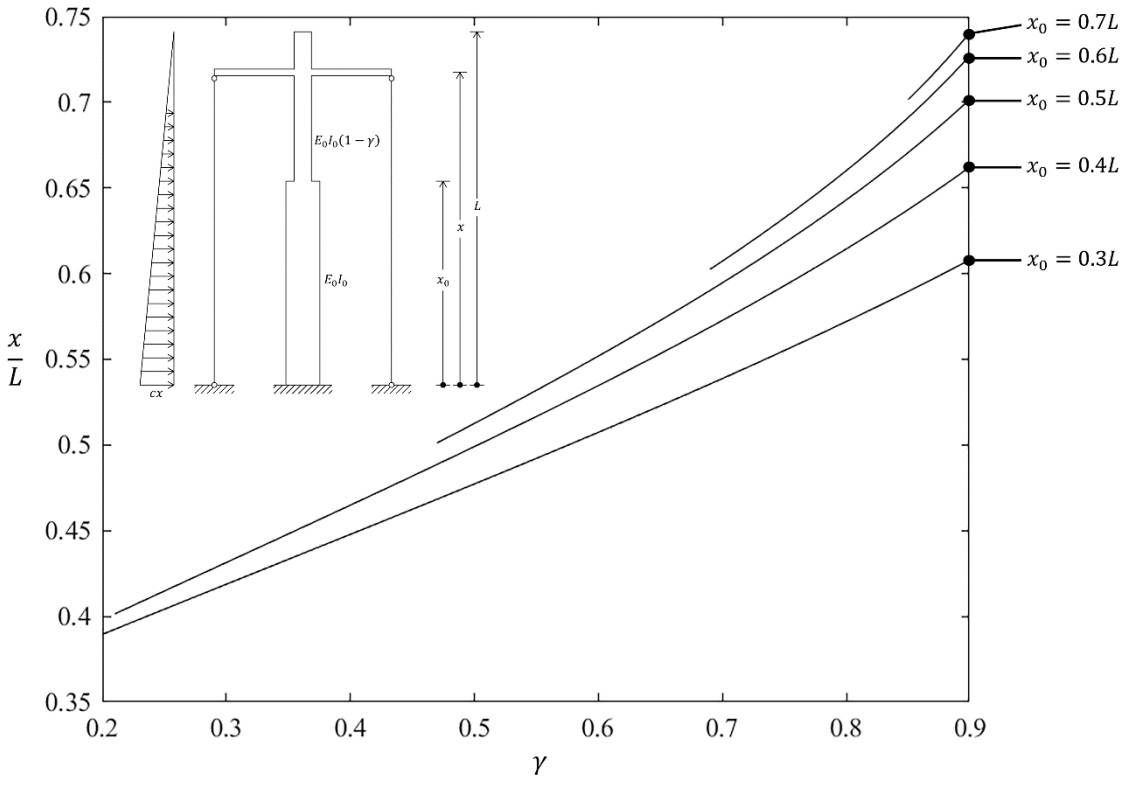

Fig. 8. Best position of CO system for inverted triangular distributed load.

In Eq. (37), assuming $x_0 = 0$ and solving Eq. (29), the position $x = 0.32L$ for the CO has been obtained, which is the position of the rigid CO with a uniform shear core. The position of the CO varies between *0.38L* and *0.74L* for different points of bending discontinuity. By increasing the value of γ (which corresponds to an increase in the slenderness of the structure's second part), the CO's position moves to the top of the structure. In Figure 8, for some values of γ, the position of the CO is located in the first part of the shear core, in which case Eq. (37) has been expressed as follows:

$$\theta(x) = E_0 I_{eq}\left(-\frac{cL^3 x}{3E_0 I_0} + \frac{cL^2 x^2}{4E_0 I_0} - \frac{q^{[3]}(x)}{E_0 I_0}\right)/(E_0 I_{eq} + AEd^2/2) \quad (38)$$

By replacing Eqs (28) and (38) in Eq. (29), the position $0.32L$has been obtained.

5.4. Parabolic distributed load

By considering the boundary conditions the coefficients of Eq. (14):

$$c_1 = 0, c_2 = 0, c_3 = \frac{wL^4}{8E_0 I_0}, c_4 = -\frac{wL^3}{18E_0 I_0} \quad (39)$$

Substituting Eq. (39) in Eq. (14), $\theta_1(x)$ becomes:

$$\theta_1(x) = -\frac{wL^4}{8E_0 I_0}\left[x + \frac{\gamma}{1-\gamma}(x - x_0)U(x - x_0)\right] + \frac{wL^3}{18E_0 I_0}\left[x^2 + \frac{\gamma}{1-\gamma}(x^2 - x_0^2)U(x - x_0)\right] - \frac{q^{[3]}(x)}{E_0 I_0} - \frac{\gamma}{1-\gamma}\frac{q^{[3]}(x) - q^{[3]}(x_0)}{E_0 I_0}U(x - x_0) \quad (40)$$

By replacing Eqs. (23) and (40) in Eq. (19):

$$\theta(x) = E_0 I_{eq}\left(-\frac{wL^4}{8E_0 I_0}\left[x + \frac{\gamma}{1-\gamma}(x - x_0)U(x - x_0)\right] + \frac{wL^3}{18E_0 I_0}\left[x^2 + \frac{\gamma}{1-\gamma}(x^2 - x_0^2)U(x - x_0)\right] - \frac{q^{[3]}(x)}{E_0 I_0} - \frac{\gamma}{1-\gamma}\frac{q^{[3]}(x) - q^{[3]}(x_0)}{E_0 I_0}U(x - x_0)\right)/(E_0 I_{eq} + AEd^2/2) \quad (41)$$

Synthesizing Eqs. (28), (29) and (41), the graph of Figure 9 has been drawn for parabolic load.

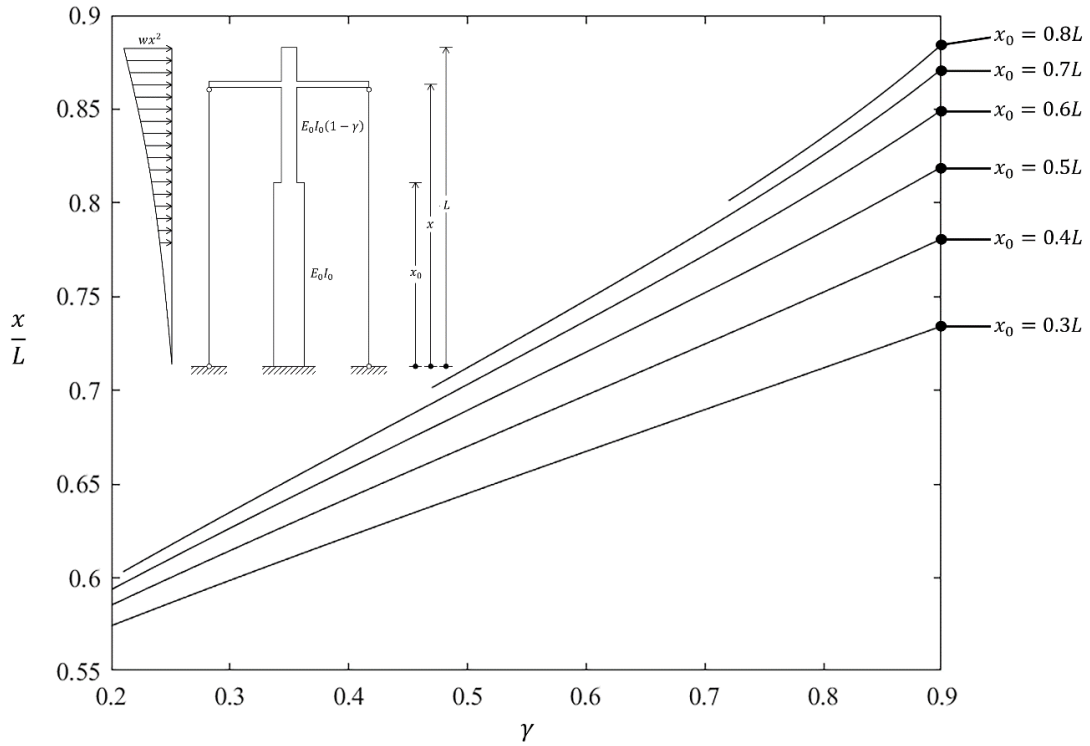

Fig. 9. Best position of CO system for parabolic distributed load.

In Eq. (41), assuming $x_0 = 0$ and solving Eq. (29), the position $x = 0.52L$ for the CO has been obtained, which is the position of the rigid CO with a uniform shear core. The position of the CO varies between *0.57L* and *0.88L* for different points of bending discontinuity. By increasing the value of γ (which corresponds to an increase in the slenderness of the structure's second part), the CO's position moves to the top of the structure. In Figure 9, for some values of γ, the position of the CO is located in the first part of the shear core, in which case Eq. (41) is expressed as follows:

$$\theta(x) = E_0 I_{eq}\left(-\frac{wL^4 x}{8E_0 I_0} + \frac{wL^3 x^2}{18E_0 I_0} - \frac{q^{[3]}(x)}{E_0 I_0}\right)/(E_0 I_{eq} + AEd^2/2) \quad (42)$$

By substituting Eqs. (28) and (42) in Eq. (29), position $0.52L$ has been obtained.

6. Conclusions

In this study, a closed-form solution based on the equivalent cross-section and the energy method was developed to determine the best positioning of CO system with step jump in the shear core's moment of inertia in tall buildings. The main findings can be summarized as follows:

When the discontinuity originates at the base of the structure (i.e., the section has no discontinuity in its moment of inertia), the best locations of the CO systems were obtained for different lateral loading conditions. For uniform, triangular, inverted triangular, and parabolic load distributions, the best locations were found to be approximately 0.44L, 0.49L, 0.32L, and 0.52L, respectively, where L is the total building height.

With an increase in the parameter γ, which reflects the greater slenderness of the upper segment of the shear core, the best positions of the CO systems shift progressively toward the upper portion of the building.

For certain values of γ, the best location of the CO falls within the first segment of the shear core, which coincides with the best location obtained for a uniform shear core.

Using closed-form solution not only ensures good accuracy in identifying the best locations but also simplifies the algebraic expressions and significantly reduces the computation time compared with numerical methods.

Overall, the proposed closed-form solution and the derived utility graphs provide a reliable and efficient tool for the preliminary design of tall buildings with discontinuous shear cores.

Funding

Our research is independent and not influenced by external factors such as financial resources, personal or professional relationships, and political affiliations.

Conflicts of interest

The authors confirm that there is no conflict of interest.

Authors contribution statement

Hamed Fallahi: Conceptualization; Data curation; Formal analysis; Investigation; Methodology; Project administration; Resources; Software; Validation; Visualization; Roles/Writing – original draft; Writing – review & editing.

Reza Rahgozar: Conceptualization; Data curation; Formal analysis; Investigation; Methodology; Project administration; Resources; Software; Supervision; Validation; Visualization; Roles/Writing – original draft; Writing – review & editing.

Yasser Sharifi: Conceptualization; Data curation; Formal analysis; Investigation; Methodology; Project administration; Resources; Supervision; Validation; Visualization.

References

[1] Hemmati A, Kheyroddin A. Behavior of large-scale bracing system in tall buildings subjected to earthquake loads. J Civ Eng Manag 2013;19:206–16.

[2] Kheyroddin A, Abdollahzadeh D, Mastali M. Improvement of open and semi-open core wall system in tall buildings by closing of the core section in the last story. Int J Adv Struct Eng 2014;6:1–12.

[3] Angelucci G, Cecca E, Mollaioli F. Parametric Analysis of Outrigger Systems for High-Rise Buildings with Different Geometric Shapes. Appl Sci 2025;15:5643.

[4] Smith B, Salim I. Parameter study of outrigger-braced tall building structures. J Struct Div 1981;107:2001–14.

[5] Smith J, Coull A, Structures TB. Analysis & Design. Wiley and sons, New York; 1991.

[6] Wu J, Li Q. Structural performance of multi-outrigger-braced tall buildings. Struct Des Tall Spec Build 2003;12:155–76.

[7] Baygi S, Khazaee A. The optimal number of outriggers in a structure under different lateral loadings. J Inst Eng Ser A 2019;100:753–61.

[8] Noormohamadian M, Salajegheh E. Multi-objective aerodynamic optimization of the exterior shape of tall buildings with trilateral cross-section. J Rehabil Civ Eng 2022;10:129–45.

[9] Chen Y, Zhang Z. Analysis of outrigger numbers and locations in outrigger braced structures using a multiobjective genetic algorithm. Struct Des Tall Spec Build 2018;27:e1408.

[10] Xing L, Gardoni P, Yu J, Zhou Y, Zhang P. Multi-objective optimization of high-rise buildings with outrigger systems subject to seismic loads. J Build Eng 2025:113197.

[11] Üstüner B, Doğan E. Weight optimization of outrigger-braced high-rise steel frames considering soil-structure interaction via metaheuristic algorithms. Structures, vol. 79, Elsevier; 2025, p. 109567.

[12] Park HS, Lee E, Choi SW, Oh BK, Cho T, Kim Y. Genetic-algorithm-based minimum weight design of an outrigger system for high-rise buildings. Eng Struct 2016;117:496–505.

[13] Habrah A, Batikha M, Vasdravellis G. An analytical optimization study on the core-outrigger system for efficient design of tall buildings under static lateral loads. J Build Eng 2022;46:103762.

[14] Babaeia M, Mohammadi Y, Ghannadiasl A. Dynamic Analysis of Tapered Tall Buildings with Different Tube Structural Systems. J Rehabil Civ Eng 2021;9:37–61.

[15] Rahgozar P. Free vibration of tall buildings using energy method and Hamilton's principle. Civ Eng J 2020;6:945–53.

[16] Kwan A. Simple method for approximate analysis of framed tube structures. J Struct Eng 1994;120:1221–39.

[17] Rahgozar R, Ahmadi A, Sharifi Y. A simple mathematical model for approximate analysis of tall buildings. Appl Math Model 2010;34:2437–51.

[18] Rahgozar R, Ahmadi A, Ghelichi M, Goudarzi Y, Malekinejad M, Rahgozar P. Parametric stress distribution and displacement functions for tall buildings under lateral loads. Struct Des Tall Spec Build 2014;23:22–41.

[19] Kamgar R, Rahgozar R. Determination of optimum location for flexible outrigger systems in non-uniform tall buildings using energy method. Int J Optim Civ Eng 2015;5:433–44.

[20] Kamgar R, Rahgozar R. Determination of optimum location for flexible outrigger systems in tall buildings with constant cross section consisting of framed tube, shear core, belt truss and outrigger system using energy method. Int J Steel Struct 2017;17:1–8.

[21] Wang M, Nagarajaiah S, Sun F. Dynamic characteristics and responses of damped outrigger tall buildings using negative stiffness. J Struct Eng 2020;146:4020273.

[22] Shelake M. Analysis of Skyscrapers with K-StyleOutrigger Belt Truss System and ShearWalls Under Lateral Load 2025.

[23] Biondi B, Caddemi S. Closed form solutions of Euler–Bernoulli beams with singularities. Int J Solids Struct 2005;42:3027–44.

[24] Al-Ansari L. Calculating of natural frequency of stepping cantilever beam. Int J Mech Mechatronics Eng IJMME-IJENS 2012;12:59–68.

[25] Jahanshahi M, Rahgozar R. Optimum location of outrigger-belt truss in tall buildings based on maximization of the belt truss strain energy 2013.

[26] Kamgar R, Rahgozar P. Reducing static roof displacement and axial forces of columns in tall buildings based on obtaining the best locations for multi-rigid belt truss outrigger systems. Asian J Civ Eng 2019;20:759–68.